

Design of Self-supporting Surfaces

Abstract

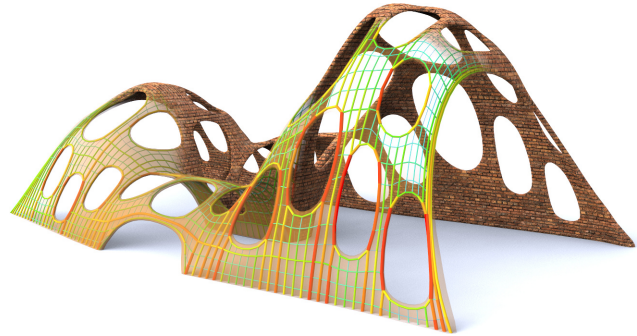


Figure 1: A surface with irregularly placed holes almost never stands by itself when built from bricks; for those that do, stability is not obvious by inspection. The surface shown is produced by finding the nearest self-supporting shape from a given freeform geometry. The image also illustrates the fictitious thrust network used in our algorithm, with edges' cross-section and coloring visualizing the magnitude of forces.

Self-supporting masonry is one of the most ancient and at the same time most elegant ways of building curved shapes. Their analysis and modeling is a topic of geometry processing rather than classical continuum mechanics, because of the very geometric nature of failure of such structures. In this paper we use the thrust network method of analysis and present an iterative nonlinear optimization algorithm for efficiently approximating freeform shapes by self-supporting ones. This provides an interactive modeling tool for such shapes. The rich geometry of thrust networks which was first studied by Maxwell in the 1860s leads us to new viewpoints of discrete differential geometry: We find close connections between different objects such as a finite-element discretization of the Airy stress potential, perfect graph Laplacians, and computing admissible loads via curvatures of polyhedral surfaces. This geometric viewpoint in particular shows us how to perform remeshing of a self-supporting shape by a self-supporting quad mesh with planar faces.

governed by the so-called Airy stress function, at least locally. This mathematical model is called a membrane in the engineering literature and has been applied to the analysis of masonry before. The surface is self-supporting if and only if stresses are entirely compressive (i.e., the Airy function is convex). For computational purposes, stresses are discretized as a fictitious *thrust network* [Block and Ochsendorf 2007] contained in the masonry structure. This is a system of forces which together with the structure's deadload is in equilibrium. It can be interpreted as a finite element discretization of the continuous case, and it turns out to have very interesting geometry dating back to the work of J. C. Maxwell [1864], with the Airy stress function becoming a polyhedral surface directly related to a reciprocal force diagram.

While previous work in architectural geometry was mostly concerned with aspects of rationalization and purely geometric side-conditions which occur in freeform architecture, the focus of this paper is design with *statics* constraints. In particular, our contributions are the following:

Contributions.

- We connect the physics of self-supporting surfaces with vertical loads to the geometry of isotropic 3-space, with the direction of gravity as the distinguished direction (§2.3). Taking the convex Airy potential as unit sphere, one can express the equations governing self-supporting surfaces in terms of curvatures.
- We employ Maxwell's construction of polyhedral thrust networks and their reciprocal diagrams (§2.4), and give an interpretation of the equilibrium conditions in terms of discrete curvatures.
- The graph Laplacian derived from a thrust network with compressive forces is a "perfect" one (§2.2). We show how it appears in the analysis and establish a connection with mean curvatures which are otherwise defined for polyhedral surfaces.
- We present an optimization algorithm for efficiently finding a thrust network near a given arbitrary reference surface (§3), and build a tool for interactive design of self-supporting surfaces based on this algorithm (§4).

Self-supporting masonry is one of the most ancient and at the same time most elegant ways of building curved shapes. Their analysis and modeling is a topic of geometry processing rather than classical continuum mechanics, because of the very geometric nature of failure of such structures. In this paper we use the thrust network method of analysis and present an iterative nonlinear optimization algorithm for efficiently approximating freeform shapes by self-supporting ones. This provides an interactive modeling tool for such shapes. The rich geometry of thrust networks which was first studied by Maxwell in the 1860s leads us to new viewpoints of discrete differential geometry: We find close connections between different objects such as a finite-element discretization of the Airy stress potential, perfect graph Laplacians, and computing admissible loads via curvatures of polyhedral surfaces. This geometric viewpoint in particular shows us how to perform remeshing of a self-supporting shape by a self-supporting quad mesh with planar faces.

CR Categories: I.3.5 [Computer Graphics]: Computational Geometry and Object Modeling—Curve, surface, solid, and object representations;

Keywords: Discrete differential geometry, architectural geometry, self-supporting masonry, thrust networks, reciprocal force diagrams, discrete Laplace operators, isotropic geometry, mean curvature

1 Introduction

Vaulted masonry structures are among the simplest and at the same time most elegant solutions for creating curved shapes in building construction. This is the reason why they have been an object of interest since antiquity, large non-convex examples being provided by gothic cathedrals. They continue to be an active topic of research in today's engineering community.

Our paper is concerned with a combined geometry+statics analysis of *self-supporting* masonry and with tools for the interactive modeling of freeform self-supporting structures. Here "self-supporting" means that the structure, considered as an arrangement of blocks (bricks, stones), holds together by itself, and additional support, additional chains and similar are present only during construction. Our analysis is based on the following assumptions, which follow the classic [Heyman 1966]:

Assumption 1: Masonry has no tensile strength, but the individual building blocks do not slip against each other (because of friction or mortar). On the other hand, their compressive strength is sufficiently high so that failure of the structure is by a sudden change in geometry, such as shown by Figure 2, and not by material failure.

Assumption 2 (The Safe Theorem): If a system of forces can be found which is in equilibrium with the load on the structure and which is contained within the masonry envelope then the structure will carry the loads, although the actually occurring forces may not be those postulated.

Our approach is twofold: We first give an overview of the continuous case of a smooth surface under stress which turns out to be

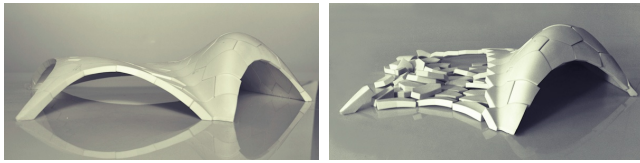


Figure 2: Masonry fails via geometric catastrophe rather than material failure (models by Block Research Group, ETH Zürich).

- We exploit the geometric relationships between a self-supporting surface and its stress potential in order to find particularly nice families of self-supporting surfaces, especially planar quadrilateral representations of thrust networks (§5).
- We demonstrate the versatility and applicability of our approach to the design and analysis of large-scale masonry and steel-glass structures.

Related Work. Unsupported masonry has been an active topic of research in the engineering community. The foundations for the modern approach were laid by Jacques Heyman [1966] and are available as the textbook [Heyman 1995]. A unifying view on polyhedral surfaces, compressive forces and corresponding “convex” force diagrams is presented by [Ash et al. 1988]. F. Fraternali [2002], [2010] established a connection between the continuous theory of stresses in membranes and the discrete theory of forces in thrust networks, by interpreting the latter as a certain non-conforming finite element discretization of the former.

Several authors have studied the problem of finding discrete compressive force networks contained within the boundary of masonry structures; early work in this area includes [Schek 1974], [Livesley 1992], and [O’Dwyer 1998]. Fraternali [2010] proposed solving for the structure’s discrete stress surface, and examining its convex hull to study the structure’s stability and susceptibility to cracking. Philippe Block’s seminal thesis introduced the method of *Thrust Network Analysis*, which linearizes the form-finding problem by first seeking a reciprocal diagram of the top view, which guarantees equilibrium of horizontal forces, then solving for the heights that balance the vertical loads (see e.g. [Block and Ochsendorf 2007; Block 2009]). Recent work by Block and coauthors extends this method in the case where the reciprocal diagram is not unique; for different choices of reciprocal diagram, the optimal heights can be found using the method of least squares [Van Mele and Block 2011], and the search for the best such reciprocal diagram can be automated using a genetic algorithm [Block and Lachauer 2011].

Other approaches to the interactive design of self-supporting structures include modeling these structures as damped particle-spring systems [Kilian and Ochsendorf 2005; Barnes 2009], and mirroring the rich tradition in architecture of designing self-supporting surfaces using hanging chain models [Heyman 1998]. Alternatively, masonry structures can be represented by networks of rigid blocks [Whiting et al. 2009], whose conditions on the structural feasibility were incorporated into procedural modeling of buildings.

Algorithmic and mathematical methods relevant to this paper are work on the geometry of quad meshes with planar faces [Glymph et al. 2004; Liu et al. 2006], discrete curvatures for such meshes [Pottmann et al. 2007; Bobenko et al. 2010], in particular curvatures in isotropic geometry [Pottmann and Liu 2007]. Schiftner and Balzer [2010] discuss approximating a reference surface by a quad mesh with planar faces, whose layout is guided by statics properties of that surface.

2 Self-supporting Surfaces

2.1 The Continuous Theory

We are here modeling masonry as a surface given by a height field $s(x, y)$ defined in some planar domain Ω . We assume that there are vertical loads $F(x, y)$ — usually F represents the structure’s own weight. By definition this surface is self-supporting, if and only if there exists a field of compressive stresses which are in equilibrium with the acting forces. This is equivalent to existence of a field $M(x, y)$ of 2×2 symmetric positive semidefinite matrices satisfying

$$\operatorname{div}(M \nabla s) = F, \quad \operatorname{div} M = 0, \quad (1)$$

where the divergence operator $\operatorname{div} \begin{pmatrix} u(x, y) \\ v(x, y) \end{pmatrix} = u_x + v_y$ is understood to act on the columns of a matrix (see e.g. [Fraternali 2010], [Giaquinta and Giusti 1985]).

The condition $\operatorname{div} M = 0$ says that M is essentially the Hessian of a real-valued function ϕ (the *Airy stress potential*): With the notation

$$M = \begin{pmatrix} m_{11} & m_{12} \\ m_{12} & m_{22} \end{pmatrix} \iff \widehat{M} = \begin{pmatrix} m_{22} & -m_{12} \\ -m_{12} & m_{11} \end{pmatrix}$$

it is clear that $\operatorname{div} M = 0$ is an integrability condition for \widehat{M} , so locally there is a potential ϕ with

$$\widehat{M} = \nabla^2 \phi, \quad \text{i.e.,} \quad M = \widehat{\nabla^2 \phi}.$$

If the domain Ω is simply connected, this relation holds globally. Positive semidefiniteness of M (or equivalently of \widehat{M}) characterizes *convexity* of the Airy potential ϕ . The Airy function enters computations only by way of its derivatives, so global existence is not an issue.

Remark: Stresses at boundary points depend on the way the surface is anchored: A fixed anchor means no condition, but a free boundary with outer normal vector \mathbf{n} means $\langle M \nabla s, \mathbf{n} \rangle = 0$.

Stress Laplacian. Note that $\operatorname{div} M = 0$ yields $\operatorname{div}(M \nabla s) = \operatorname{tr}(M \nabla^2 s)$, which we like to call $\Delta_\phi s$. The operator Δ_ϕ is symmetric. It is elliptic (as a Laplace operator should be) if and only if M is positive definite, i.e., ϕ is strictly convex. The balance condition (1) may be written as $\Delta_\phi s = F$.

2.2 Discrete Theory: Thrust Networks

We are discretizing a self-supporting surface by a mesh $\mathcal{S} = (V, E, F)$ (see Figure 3). Loads are again vertical, and we discretize them as force densities F_i associated with vertices \mathbf{v}_i . The load acting on this vertex is then given by $F_i A_i$, where A_i is an area of influence (using a prime to indicate projection onto the xy plane, A_i is the area of the Voronoi cell of \mathbf{v}'_i w.r.t. V'). We assume that stresses are carried by the edges of the mesh: the force exerted on the vertex \mathbf{v}_i by the edge connecting $\mathbf{v}_i, \mathbf{v}_j$ is given by

$$w_{ij}(\mathbf{v}_j - \mathbf{v}_i), \quad \text{where} \quad w_{ij} = w_{ji} \geq 0.$$

The nonnegativity of the individual weights w_{ij} expresses the compressive nature of forces. The balance conditions at vertices then read as follows: With $\mathbf{v}_i = (x_i, y_i, s_i)$ we have

$$\sum_{j \sim i} w_{ij}(x_j - x_i) = \sum_{j \sim i} w_{ij}(y_j - y_i) = 0, \quad (2)$$

$$\sum_{j \sim i} w_{ij}(s_j - s_i) = A_i F_i. \quad (3)$$

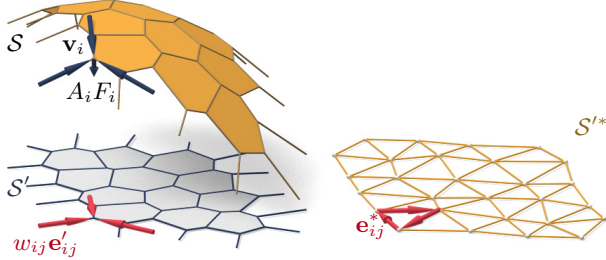


Figure 3: A thrust network \mathcal{S} , with dangling edges indicating external forces (left). This network together with compressive forces which balance vertical loads $A_i F_i$ projects onto a planar mesh \mathcal{S}' with equilibrium compressive forces $w_{ij} \mathbf{e}'_{ij}$ in its edges. Rotating forces by 90° leads to the reciprocal force diagram \mathcal{S}'^* (right).

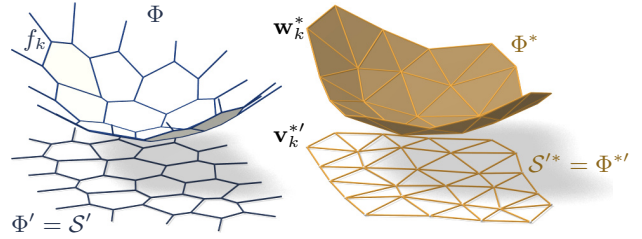


Figure 4: Airy stress potential Φ and its polar dual Φ^* . Φ projects onto the same planar mesh as \mathcal{S} does, while Φ^* projects onto the reciprocal force diagram. A primal face f_k lies in the plane $z = \alpha x + \beta y + \gamma \iff$ the corresponding dual vertex is $\mathbf{w}_k^* = (\alpha, \beta, -\gamma)$.

181 A mesh equipped with edge weights in this way is a discrete *thrust* 182 network. Invoking the safe theorem, we can state that a masonry 183 structure is self-supporting, if we can find a thrust network with 184 compressive forces which is entirely contained within the structure.

185 **Reciprocal Diagram.** Equations (2) have a geometric interpretation: With edge vectors 186

$$\mathbf{e}'_{ij} = \mathbf{v}'_j - \mathbf{v}'_i = (x_j, y_j) - (x_i, y_i),$$

187 Equation (2) asserts that vectors $w_{ij} \mathbf{e}'_{ij}$ form a closed cycle. Rotating them by 90 degrees, we see that likewise 188

$$\mathbf{e}'_{ij}^* = w_{ij} J \mathbf{e}'_{ij}, \quad \text{with } J = \begin{pmatrix} 0 & -1 \\ 1 & 0 \end{pmatrix},$$

189 form a closed cycle (see Figure 3). If the mesh \mathcal{S} is simply connected, there exists an entire *reciprocal diagram* \mathcal{S}'^* which is a 190 combinatorial dual of \mathcal{S} , and which has edge vectors \mathbf{e}'_{ij}^* . Its 191 vertices are denoted by \mathbf{v}'^*_i . 192

193 *Remark:* If \mathcal{S}' is a Delaunay triangulation, then the corresponding 194 Voronoi diagram is an example of a reciprocal diagram.

195 **Polyhedral Stress Potential.** We can go further and construct a 196 convex polyhedral “Airy stress potential” surface Φ with vertices 197 $\mathbf{w}_i = (x_i, y_i, \phi_i)$ combinatorially equivalent to \mathcal{S} by requiring that 198 a primal face of Φ lies in the plane $z = \alpha x + \beta y + \gamma$ if and only if 199 (α, β) is the corresponding dual vertex of \mathcal{S}'^* (see Figure 4). Ob- 200viously this condition determines Φ up to vertical translation. For 201 existence see [Ash et al. 1988]. The inverse procedure constructs 202 a reciprocal diagram from Φ . This procedure works also if forces 203 are not compressive: we can construct an Airy mesh Φ which has 204 planar faces, but it will no longer be a convex polyhedron.

205 The vertices of Φ can be interpolated by a piecewise-linear function 206 $\phi(x, y)$. It is easy to see that the derivative of $\phi(x, y)$ jumps by the 207 amount $\|\mathbf{e}'_{ij}^*\| = w_{ij} \|\mathbf{e}'_{ij}\|$, when crossing over the edge \mathbf{e}'_{ij} at right 208 angle, with unit speed. This identifies Φ as the Airy polyhedron in- 209 troduced by [Fraternali et al. 2002] as a finite element discretization 210 of the continuous Airy function (see also [Fraternali 2010]).

211 If the mesh is not simply connected, the reciprocal diagram and the 212 Airy polyhedron exist only locally. Global existence is not an issue 213 for our computations.

214 **Polarity.** Polarity with respect to the *Maxwell paraboloid* $z =$ 215 $\frac{1}{2}(x^2 + y^2)$ maps the plane $z = \alpha x + \beta y + \gamma$ to the point $(\alpha, \beta, -\gamma)$. 216 Thus, applying polarity to Φ and projecting the result Φ^* into the xy 217 plane reconstructs the reciprocal diagram $\Phi'^* = \mathcal{S}'^*$ (see Fig. 4).

218 **Discrete Stress Laplacian.** The weights w_{ij} may be used to de- 219 fine a graph Laplacian Δ_ϕ which on vertex-based functions acts as

$$\Delta_\phi s(\mathbf{v}_i) = \sum_{j \sim i} w_{ij} (s_j - s_i).$$

220 This operator is a perfect discrete Laplacian in the sense of [War- 221 detzky et al. 2007], since it is symmetric by construction, Equa- 222 tion (2) implies linear precision for the planar “top view mesh” \mathcal{S}' 223 (i.e., $\Delta_\phi f = 0$ if f is a linear function), and $w_{ij} \geq 0$ ensures 224 semidefiniteness and a maximum principle for Δ_ϕ -harmonic func- 225 tions. Equation (3) can be written as $\Delta_\phi s = AF$.

226 Note that Δ_ϕ is well defined also in case the underlying meshes are 227 not simply connected.

2.3 Surfaces in Isotropic Geometry

228 It is worth while to reconsider the basics of self-supporting surfaces 229 in the language of dual-isotropic geometry, which takes place in \mathbb{R}^3 230 with the z axis as a distinguished vertical direction. The basic ele- 231 ments of this geometry are planes, having equation $z = f(x, y) =$ 232 $\alpha x + \beta y + \gamma$. The gradient vector $\nabla f = (\alpha, \beta)$ determines the 233 plane up to translation. A plane tangent to the graph of the function 234 $s(x, y)$ has gradient vector ∇s .

235 There is the notion of *parallel points*: $(x, y, z) \parallel (x', y', z') \iff$ 236 $x = x', y = y'$.

237 *Remark:* The Maxwell paraboloid is considered the unit sphere of 238 isotropic geometry, and the geometric quantities considered above 239 are assigned specific meanings: The forces $\|\mathbf{e}'_{ij}^*\| = w_{ij} \|\mathbf{e}'_{ij}\|$ are 240 dihedral angles of the Airy polyhedron Φ , and also “lengths” of 241 edges of Φ^* . We do not use this terminology in the sequel.

242 **Curvatures.** Generally speaking, in the differential geometry of 243 surfaces one considers the *Gauss map* σ from a surface S to a con- 244 vex unit sphere Φ by requiring that corresponding points have par- 245 allel tangent planes. Subsequently mean curvature H^{rel} and Gaus- 246 sian curvature K^{rel} relative to Φ are computed from the derivative 247 $d\sigma$. Classically Φ is the ordinary unit sphere $x^2 + y^2 + z^2 = 1$, so 248 that σ maps each point its unit normal vector.

249 In our setting, parallelity is a property of *points* rather than planes, 250 and the Gauss map σ goes the other way, mapping the tangent 251 planes of the unit sphere $z = \phi(x, y)$ to the corresponding tan- 252 gent plane of the surface $z = s(x, y)$. If we know which point a 253 plane is attached to, then it is determined by its gradient. So we 254 simply write

$$\nabla \phi \xrightarrow{\sigma} \nabla s.$$

By moving along a curve $\mathbf{u}(t) = (x(t), y(t))$ in the parameter domain we get the first variation of tangent planes: $\frac{d}{dt} \nabla \phi|_{\mathbf{u}(t)} = (\nabla^2 \phi)\dot{\mathbf{u}}$. This yields the derivative $(\nabla^2 \phi)\dot{\mathbf{u}} \stackrel{d\sigma}{\mapsto} (\nabla^2 s)\dot{\mathbf{u}}$, for all $\dot{\mathbf{u}}$, and the matrix of $d\sigma$ is found as $(\nabla^2 \phi)^{-1}(\nabla^2 s)$. By definition, curvatures of the surface s relative to ϕ are found as

$$K_s^{\text{rel}} = \det(d\sigma) = \frac{\det \nabla^2 s}{\det \nabla^2 \phi},$$

$$H_s^{\text{rel}} = \frac{1}{2} \text{tr}(d\sigma) = \frac{1}{2} \text{tr} \left(\frac{M}{\det \nabla^2 \phi} \nabla^2 s \right) = \frac{\Delta_\phi s}{2 \det \nabla^2 \phi}.$$

The Maxwell paraboloid $\phi_0(x, y) = \frac{1}{2}(x^2 + y^2)$ is the canonical unit sphere of isotropic geometry, its Hessian equals E_2 . Curvatures relative to ϕ_0 are not called “relative” and are denoted by the symbols H, K instead of $H^{\text{rel}}, K^{\text{rel}}$. The observation

$$\Delta_\phi \phi = \text{tr}(M \nabla^2 \phi) = \text{tr}(\widehat{\nabla^2 \phi} \nabla^2 \phi) = 2 \det \nabla^2 \phi$$

together with the formulas above implies

$$K_s = \det \nabla^2 s, \quad K_\phi = \det \nabla^2 \phi \implies H_s^{\text{rel}} = \frac{\Delta_\phi s}{2K_\phi} = \frac{\Delta_\phi s}{\Delta_\phi \phi}.$$

Relation to Self-supporting Surfaces. Summarizing the formulas above, we rewrite the balance condition (1) as

$$2K_\phi H_s^{\text{rel}} = \Delta_\phi s = F. \quad (4)$$

Let us draw some conclusions:

- Since $H_\phi^{\text{rel}} = 1$ we see that the load $F_\phi = 2K_\phi$ is admissible for the stress surface $\phi(x, y)$, which is hereby shown as self-supporting. The quotient of loads yields $H_s^{\text{rel}} = F/F_\phi$.
- If the stress surface coincides with the Maxwell paraboloid, then *constant loads characterize constant mean curvature surfaces*, because we get $K_\phi = 1$ and $H_s = F/2$.
- If s_1, s_2 have the same stress potential ϕ , then $H_{s_1-s_2}^{\text{rel}} = H_{s_1}^{\text{rel}} - H_{s_2}^{\text{rel}} = 0$, so $s_1 - s_2$ is a (relative) minimal surface.

2.4 Meshes in Isotropic Geometry

A general theory of curvatures of polyhedral surfaces with respect to a polyhedral unit sphere was proposed by [Pottmann et al. 2007; Bobenko et al. 2010], and its dual complement in isotropic geometry was elaborated by [Pottmann and Liu 2007]. As illustrated by Figure 5, the mean curvature of a self-supporting surface \mathcal{S} relative to its discrete Airy stress potential is associated with the vertices of \mathcal{S} . It is computed from areas and mixed areas of faces in the polar polyhedra \mathcal{S}^* and Φ^* :

$$H^{\text{rel}}(\mathbf{v}_i) = \frac{A_i(\mathcal{S}, \Phi)}{A_i(\Phi, \Phi)}, \quad \text{where}$$

$$A_i(\mathcal{S}, \Phi) = \frac{1}{4} \sum_{k: f_k \in 1\text{-ring}(\mathbf{v}_i)} \det(\mathbf{v}'_k, \mathbf{w}'_{k+1}) + \det(\mathbf{w}'_k, \mathbf{v}'_{k+1}).$$

The prime denotes the projection into the xy plane, and summation is over those dual vertices which are adjacent to \mathbf{v}_i . Replacing \mathbf{v}'_k by \mathbf{w}'_k yields $A_i(\Phi, \Phi) = \frac{1}{2} \sum \det(\mathbf{w}'_k, \mathbf{w}'_{k+1})$.

Proposition. If Φ is the Airy surface of a thrust network \mathcal{S} , then the mean curvature of \mathcal{S} relative to Φ is computable as

$$H^{\text{rel}}(\mathbf{v}_i) = \frac{\sum_{j \sim i} w_{ij}(s_j - s_i)}{\sum_{j \sim i} w_{ij}(\phi_j - \phi_i)} = \frac{\Delta_\phi s}{\Delta_\phi \phi}|_{\mathbf{v}_i}. \quad (5)$$

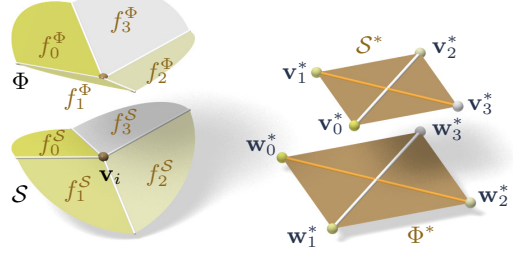


Figure 5: Mean curvature of a vertex \mathbf{v}_i of \mathcal{S} : Corresponding edges of the polar duals \mathcal{S}^* , Φ^* are parallel, and mean curvature according to [Pottmann et al. 2007] is computed from the vertices polar to faces adjacent to \mathbf{v}_i . For valence 4 vertices the case of zero mean curvature shown here is characterized by parallelity of non-corresponding diagonals of corresponding quads in \mathcal{S}^* , Φ^* .

Proof. It is sufficient to show $2A_i(\mathcal{S}, \Phi) = \sum_{j \sim i} w_{ij}(s_j - s_i)$.

For that, consider edges $\mathbf{e}'_1, \dots, \mathbf{e}'_n$ emanating from \mathbf{v}'_i . The dual cycles in Φ^* and \mathcal{S}^* without loss of generality are given by vertices $(\mathbf{v}'_1, \dots, \mathbf{v}'_n)$ and $(\mathbf{w}'_1, \dots, \mathbf{w}'_n)$, respectively. The latter has edges $\mathbf{w}'_{j+1} - \mathbf{w}'_j = w_{ij} \mathbf{J} \mathbf{e}'_j$ (indices modulo n).

Without loss of generality $\mathbf{v}_i = 0$, so the vertex \mathbf{v}'_j by construction equals the gradient of the linear function $\mathbf{x} \mapsto \langle \mathbf{v}'_j, \mathbf{x} \rangle$ defined by the properties $\mathbf{e}'_{j-1} \mapsto s_{j-1} - s_i, \mathbf{e}'_j \mapsto s_j - s_i$. Corresponding edge vectors $\mathbf{v}'_{j+1} - \mathbf{v}'_j$ and $\mathbf{w}'_{j+1} - \mathbf{w}'_j$ are parallel, because $\langle \mathbf{v}'_{j+1} - \mathbf{v}'_j, \mathbf{e}'_j \rangle = (s_j - s_i) - (s_j - s_i) = 0$. Expand $2A_i(\mathcal{S}, \Phi)$:

$$\begin{aligned} & \frac{1}{2} \sum \det(\mathbf{w}'_j, \mathbf{v}'_{j+1}) + \det(\mathbf{v}'_j, \mathbf{w}'_{j+1}) \\ &= \frac{1}{2} \sum \det(\mathbf{w}'_j - \mathbf{w}'_{j+1}, \mathbf{v}'_{j+1}) + \det(\mathbf{v}'_j, \mathbf{w}'_{j+1} - \mathbf{w}'_j) \\ &= \frac{1}{2} \sum \det(-w_{ij} \mathbf{J} \mathbf{e}'_j, \mathbf{v}'_{j+1}) + \det(\mathbf{v}'_j, w_{ij} \mathbf{J} \mathbf{e}'_j) \\ &= \sum \det(\mathbf{v}'_j, w_{ij} \mathbf{J} \mathbf{e}'_j) = \sum w_{ij} \langle \mathbf{v}'_j, \mathbf{e}'_j \rangle = \sum w_{ij} (s_j - s_i). \end{aligned}$$

Here we have used $\det(\mathbf{a}, \mathbf{J} \mathbf{b}) = \langle \mathbf{a}, \mathbf{b} \rangle$. \square

In order to discretize (4), we also need a discrete Gaussian curvature, which is usually defined as a quotient of areas which correspond under the Gauss mapping. We define

$$K_\Phi(\mathbf{v}_i) = \frac{A_i(\Phi, \Phi)}{A_i},$$

where A_i is the Voronoi area of vertex \mathbf{v}'_i in the projected mesh \mathcal{S}' used in (3).

Remark: If the faces of the thrust network \mathcal{S} are not planar, the simple trick of introducing additional edges with zero forces in them makes them planar, and the theory is applicable. We refrain from elaborating this further.

Discrete Balance Equation. The discrete version of the balance equation (4) reads as follows:

Theorem. A simply-connected mesh \mathcal{S} with vertices $\mathbf{v}_i = (x_i, y_i, s_i)$ can be put into static equilibrium with vertical forces “ $A_i F_i$ ” if and only if there exists a combinatorially equivalent mesh Φ with planar faces and vertices (x_i, y_i, ϕ_i) , such that curvatures of \mathcal{S} relative to Φ obey

$$2K_\Phi(\mathbf{v}_i) H^{\text{rel}}(\mathbf{v}_i) = F_i \quad (6)$$

at every interior vertex and every free boundary vertex \mathbf{v}_i . \mathcal{S} can be put into compressive static equilibrium if and only if there exists a convex such Φ .

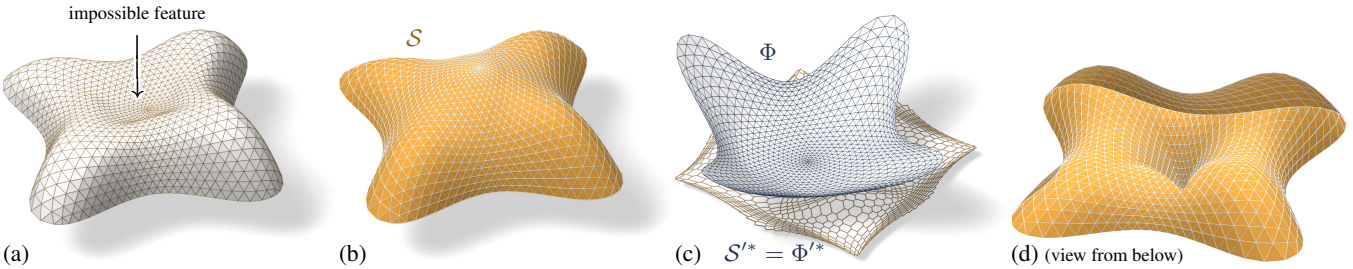


Figure 6: The top of the Lilium Tower (a) cannot stand as a masonry structure, because its central part is concave. Our algorithm finds a nearby self-supporting mesh (b) without this impossible feature. (c) shows the corresponding Airy mesh Φ and reciprocal force diagram S'^* . (d) The user can edit the original surface, such as by specifying that the center of the surface is supported by a vertical pillar; and the self-supporting network adjusts accordingly.

Proof. The relation between equilibrium forces $w_{ij}\mathbf{e}_{ij}$ in \mathcal{S} and the polyhedral stress potential Φ has been discussed above, and so has the equivalence “ $w_{ij} \geq 0 \iff \Phi$ convex” (see e.g. [Ash et al. 1988] for a survey of this and related results). It remains to show that Equations (2) and (6) are equivalent. This is the case because the proposition above implies $2K(\mathbf{v}_i)H^{\text{rel}}(\mathbf{v}_i) = 2\frac{A_i(\Phi, \Phi)}{A_i} = \frac{1}{A_i}(\sum_{j \sim i} w_{ij}(s_j - s_i)) = \frac{1}{A_i}A_iF_i$. \square

Existence of Discretizations. When considering discrete thrust networks as discretizations of continuous self-supporting surfaces, the following question is important: For a given smooth surface $s(x, y)$ with Airy stress function ϕ , does there exist a polyhedral surface \mathcal{S} in equilibrium approximating $s(x, y)$, whose top view is a given planar mesh \mathcal{S}' ? We restrict our attention to triangle meshes, where planarity of the faces of the discrete stress surface Φ is not an issue. This question has several equivalent reformulations:

- Does \mathcal{S}' have a reciprocal diagram whose corresponding Airy polyhedron Φ approximates the continuous Airy potential ϕ ? (if the surfaces involved are not simply connected, these objects are defined locally).
- Does \mathcal{S}' possess a “perfect” discrete Laplace-Beltrami operator Δ_ϕ in the sense of Wardetzky et al. [2007] whose weights are the edge length scalars of such a reciprocal diagram?

From [Wardetzky et al. 2007] we know that perfect Laplacians exist only on regular triangulations which are projections of convex polyhedra. On the other hand, previous sections show how to appropriately re-triangulate: Let Φ be a triangle mesh convex hull of the vertices $(x_i, y_i, \phi(x_i, y_i))$, where (x_i, y_i) are vertices of \mathcal{S}' . Then its polar dual Φ^* projects onto a reciprocal diagram with positive edge weights, so Δ_ϕ has positive weights, and the vertices (x_i, y_i, s_i) of \mathcal{S} can be found by solving the discrete Poisson problem $(\Delta_\phi s)_i = A_iF_i$.

Assuming the discrete Δ_ϕ approximates its continuous counterpart, this yields a mesh approximating $s(x, y)$, and we conclude: A smooth self-supporting surface can be approximated by a discrete self-supporting triangular mesh for any sampling of the surface.

3 Thrust Networks from Reference Meshes

Consider now the problem of taking a given reference mesh, say \mathcal{R} , and finding a combinatorially equivalent mesh \mathcal{S} in static equilibrium approximating \mathcal{R} . The loads on \mathcal{S} include user-prescribed loads as well as the dead load caused by the mesh’s own weight. Conceptually, finding \mathcal{S} amounts to minimizing some formulation of distance between \mathcal{R} and \mathcal{S} , subject to constraints (2), (3), and $w_{ij} \geq 0$. For any choice of distance this minimization will be a nonlinear, non-convex, inequality-constrained variational problem

that cannot be efficiently solved in practice. Instead we propose a staggered optimization algorithm:

0. Start with an initial guess $\mathcal{S} = \mathcal{R}$.
1. Estimate the self-load on the vertices of \mathcal{S} , using their current positions.
2. Fixing \mathcal{S} , fit an associated stress surface Φ .
3. Alter positions \mathbf{v}_i to improve the fit.
4. Repeat from Step 1 until convergence.

Step 1: Estimating Self-Load. The dead load due to the surface’s own weight depends not only on the top view of \mathcal{S} , but also on the surface area of its faces. To avoid adding nonlinearity to the algorithm, we estimate the load coefficients F_i at the beginning of each iteration, and assume they remain constant until the next iteration. We estimate the load “ A_iF_i ” associated with each vertex by calculating its Voronoi area on each of its incident faces, and then multiplying by a user-specified surface density ρ .

Step 2: Fit a Stress Surface. In this step, we fix \mathcal{S} and try to fit a stress surface Φ subordinate to the top view \mathcal{S}' of the primal mesh. We do so by searching for dihedral angles between the faces of Φ which minimize, in the least-squares sense, the error in force equilibrium (6) and local integrability of Φ . Doing so is equivalent to minimizing the squared residuals of Equations (3) and (2), respectively, with the positions held fixed. Defining the *equilibrium energy*

$$E = \sum_i \left\| \begin{pmatrix} 0 \\ 0 \\ A_iF_i \end{pmatrix} - \sum_{j \sim i} w_{ij}(\mathbf{v}_j - \mathbf{v}_i) \right\|^2, \quad (7)$$

where the outer sum is over the interior and free boundary vertices, we solve

$$\min_{w_{ij}} E, \quad \text{s.t. } 0 \leq w_{ij} \leq w_{\max}. \quad (8)$$

Here w_{\max} is an optional maximum weight we are willing to assign (to limit the amount of stress in the surface). This convex, sparse, box-constrained least-squares problem [Friedlander 2007] always has a solution. If the objective is 0 at this solution, the faces of Φ locally integrate to a stress surface satisfying (6), and so Φ certifies that \mathcal{S} is self-supporting – we are done. Otherwise, \mathcal{S} is not self-supporting and its vertices must be moved.

Step 3: Alter Positions. In the previous step we fit as best as possible a stress surface Φ to \mathcal{S} . There are two possible kinds of error with this fit: the faces around a vertex (equivalently, the reciprocal diagram) might not close up; and the resulting stress forces might not be exactly in equilibrium with the loads. These errors



Figure 7: The user-designed reference mesh (left) is not self-supporting, but our algorithm finds a nearby perturbation of the reference surface (middle-left) that is in equilibrium. As the user makes edits to the reference surface (middle-right), the thrust network automatically adjusts (right).

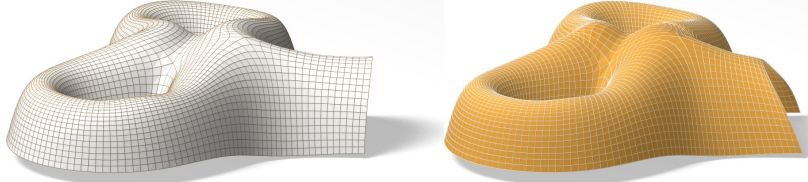


Figure 8: A freeform surface (left) needs adjustments around the entrance arch and between the two pillars in order to be self-supporting; our algorithm finds the nearby surface in equilibrium (right) that incorporates these changes.

403 can be decreased by modifying the top view and heights of \mathcal{S} , re-
404 spectively. It is possible to simply solve for new vertex positions
405 that put \mathcal{S} in static equilibrium, since Equations (2) and (3) with
406 w_{ij} fixed form a square linear system that is typically nonsingular.

407 While this approach would yield a self-supporting \mathcal{S} , this mesh is
408 often far from the reference mesh \mathcal{R} , since any local errors in the
409 stress surface from Step 2 amplify into global errors in \mathcal{S} . We pro-
410 pose instead to look for new positions that decrease the imbalance
411 in the stresses and loads, while also penalizing drift away from the
412 reference mesh:

$$\min_{\mathbf{v}} E + \alpha \sum_i \langle \mathbf{n}_i, \mathbf{v}_i - \mathbf{v}_i^0 \rangle^2 + \beta \|\mathbf{v} - \mathbf{v}_P^0\|^2,$$

413 where \mathbf{v}_i^0 is the position of the i -th vertex at the start of this step
414 of the optimization, \mathbf{n}_i is the starting vertex normal (computed as
415 the average of the incident face normals), \mathbf{v}_P^0 is the projection of \mathbf{v}^0
416 onto the reference mesh, and $\alpha > \beta$ are penalty coefficients that are
417 decreased every iteration of Steps 1–3 of the algorithm. The second
418 term allows \mathcal{S} to slide over itself (if doing so improves equilibrium)
419 but penalizes drift in the normal direction. The third term, weaker
420 than the second, regularizes the optimization by preventing large
421 drift away from the reference surface or excessive tangential slid-
422 ing.

423 **Implementation Details.** Solving the weighted least-squares
424 problem of Step 3 amounts to solving a sparse, symmetric linear
425 system. While the MINRES algorithm [Paige and Saunders 1975]
426 is likely the most robust algorithm for solving this system, in prac-
427 tice we have observed that the method of conjugate gradients works
428 well despite the potential ill-conditioning of the objective matrix.

429 **Limitations.** This algorithm is not guaranteed to always con-
430 verge; this fact is not surprising from the physics of the problem
431 (if the boundary of the reference mesh encloses too large of a re-
432 gion, w_{\max} is set too low, and the density of the surface too high,
433 a thrust network in equilibrium simply does not exist – the vault is
434 too ambitious and cannot be built to stand; pillars are needed.)

435 We can, however, make a few remarks. Step 2 always decreases the
436 equilibrium energy E of Equation (7) and Step 3 does as well as
437 $\beta \rightarrow 0$. Moreover, as $\alpha \rightarrow 0$ and $\beta \rightarrow 0$, Step 3 approaches a lin-
438 ear system with as many equations as unknowns; if this system has

439 full rank, its solution sets $E = 0$. These facts suggest that the algo-
440 rithm should generally converge to a thrust network in equilibrium,
441 provided that Step 1 does not increase the loads by too much at ev-
442 ery iteration, and this is indeed what we observe in practice. One
443 case where this assumption is guaranteed to hold is if the thickness
444 of the surface is allowed to freely vary, so that it can be chosen so
445 that the surface has uniform density over the top view.

446 If the linear system in Step 3 is singular and infeasible, the algo-
447 rithm can stall at $E > 0$. This failure occurs, for instance, when
448 an interior vertex has height z_i lower than all of its neighbors, and
449 Step 2 assigns all incident edges to that vertex a weight of zero:
450 clearly no amount of moving the vertex or its neighbors can bring
451 the vertex into equilibrium. We avoid such degenerate configura-
452 tions by bounding weights slightly away from zero in (8), trading
453 increased robustness for slight smoothing of the resulting surface.

4 Results

455 **Interactive Design of Self-Supporting Surfaces.** The opti-
456 mization algorithm described in the previous section forms the ba-
457 sis of an interactive design tool for self-supporting surfaces. Users
458 manipulate a mesh representing a reference surface, and the com-
459 puter searches for a nearby thrust network in equilibrium (see e.g.
460 Figure 7). Fitting this thrust network does not require that the user
461 specify boundary tractions, and although the top view of the refer-
462 ence mesh is used as an initial guess for the top view of the thrust
463 network, the search is not restricted to this top view. The features
464 of the design tool include:

- Handle-based 3D editing of the reference mesh using Lapla-
466 cian coordinates [Lipman et al. 2004; Sorkine et al. 2003] to
467 extrude vaults, insert pillars, and apply other deformations to
468 the reference mesh. Handle-based adjustments of the heights,
469 keeping the top view fixed, and deformation of the top view,
470 keeping the heights fixed, are also supported. The thrust net-
471 work adjusts interactively to fit the deformed positions, giving
472 the usual visual feedback about the effects of edits on whether
473 or not the surface can stand.
- Specification of boundary conditions. Points of contact be-
474 tween the reference surface and the ground or environment
475 are specified by “pinning” vertices of the surface, specifying
476 that the thrust network must coincide with the reference mesh

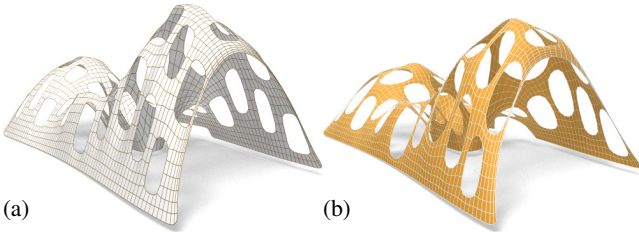


Figure 9: A mesh with holes (a) requires large deformations to both the top view and heights to render it self-supporting (b)

478 at this point, and relaxing the condition that forces must be in
479 equilibrium there.

- 480 • Interactive adjustment of surface density ρ , external loads,
481 and maximum permissible stress per edge w_{\max} , with visual
482 feedback of how these parameters affect the fitted thrust net-
483 work.
- 484 • Upsampling of the thrust network through Catmull-Clark sub-
485 division and polishing of the resulting refined thrust network
486 using optimization (§3).
- 487 • Visualization of the stress surface dual to the thrust network
488 and corresponding reciprocal diagram.

Example: Vault with Pillars. As an example of the design and optimization workflow, consider a rectangular vault with six pillars, free boundary conditions along one edge, fixed boundary conditions along the others, and a tower extruded from the top of the surface (see Figure 7). This surface is neither convex nor simply connected, and exhibits a mix of boundary conditions, none of which cause our algorithm any difficulty; it finds a self-supporting thrust network near the designed reference mesh. The user is now free to make edits to the reference mesh, and the thrust network adapts to these edits, providing the user feedback on whether these designs are physically realizable.

Example: Top of the Lilium Tower. Consider the top portion of the steel-glass exterior surface of the Lilium Tower, which is currently being built in Warszaw (see Figure 6). This surface contains a concave part with local minimum in its interior and so cannot possibly be self-supporting. Given this surface as a reference mesh, our algorithm constructs a nearby thrust network in equilibrium without the impossible feature. The user can then explore how editing the reference mesh – adding a pillar, for example – affects the thrust network and its deviation from the reference surface.

Example: Freeform Structure with Two Pillars. Suppose an architect’s experience and intuition has permitted the design of a freeform surface (see Figure 8) that is nearly self-supporting. Our algorithm reveals those edits needed to make the structure sound – principally around the entrance arch, and the area between the two pillars.

Example: Swiss Cheese. Cutting holes in a self-supporting surface interrupts force flow lines and causes dramatic global changes to the surface stresses, often to the point that the surface is no longer in equilibrium. Whether a given surface with many such holes can stand is far from obvious. Figures 9 show such an implausible and unstable surface; our optimization finds a nearby, equally implausible but stable surface without difficulty (see Figures 1 and 9).

5 Special Self-Supporting Surfaces

PQ Meshes. Meshes with *planar* faces are of particular interest in architecture, so in this section we discuss how to remesh a given thrust network in equilibrium such that it becomes a quad mesh with planar faces (again in equilibrium). If this mesh is realized as a steel-glass construction, it is self-supporting in its beams alone, with no forces exerted on the glass (this is the usual manner of using glass). The beams constitute a self-supporting structure which is in perfect force equilibrium (without moments in the nodes) if only the deadload is applied.



Figure 10: Directly enforcing planarity of the faces of even a very simple self-supporting quad-mesh vault (a) results in a surface far removed from the original design (b). Starting instead from a remeshing of the surface with edges following relative principal curvature directions yields a self-supporting, PQ mesh far more faithful to the original (c).

532 Taking an arbitrary non-planar quad mesh and attempting naive,
533 simultaneous enforcement of planarity and static equilibrium does
534 not yield good results, as shown in Figure 10. To identify the neces-
535 sary conditions, we first discuss a planar quad mesh \mathcal{S} with vertices
536 $\mathbf{v}_{ij} = (x_{ij}, y_{ij}, s_{ij})$ which approximates a given continuous sur-
537 face $s(x, y)$. It is known that \mathcal{S} must approximately follow a net-
538 work of conjugate curves in the surface (see e.g. [Liu et al. 2006]).
539 We can derive this condition in an elementary way as follows: Us-
540 ing a Taylor expansion, we compute the volume of the convex hull
541 of the quadrilateral $\mathbf{v}_{ij}, \mathbf{v}_{i+1,j}, \mathbf{v}_{i+1,j+1}, \mathbf{v}_{i,j+1}$, assuming the ver-
542 tices lie exactly on the surface $s(x, y)$. This results in

$$\text{vol} = \frac{1}{6} \det(\mathbf{a}_1, \mathbf{a}_2) \cdot ((\mathbf{a}_1)^T \nabla^2 s \mathbf{a}_2) + \dots,$$

where $\mathbf{a}_1 = \begin{pmatrix} x_{i+1,j} - x_{ij} \\ y_{i+1,j} - y_{ij} \end{pmatrix}$, $\mathbf{a}_2 = \begin{pmatrix} x_{i,j+1} - x_{ij} \\ y_{i,j+1} - y_{ij} \end{pmatrix}$,

543 and the dots indicate higher order terms. We see that planarity re-
544 quires $(\mathbf{a}_1)^T \nabla^2 s \mathbf{a}_2 = 0$. In addition to the mesh \mathcal{S} approximating
545 the surface $s(x, y)$, the corresponding polyhedral Airy surface Φ
546 must approximate $\phi(x, y)$; thus we get the conditions

$$(\mathbf{a}_1)^T \nabla^2 s \mathbf{a}_2 = (\mathbf{a}_1)^T \nabla^2 \phi \mathbf{a}_2 = 0.$$

547 $\mathbf{a}_1, \mathbf{a}_2$ are therefore eigenvectors of $(\nabla^2 \phi)^{-1} \nabla^2 s$. In view of §2.3,
548 $\mathbf{a}_1, \mathbf{a}_2$ indicate the principal directions of the surface $s(x, y)$ rela-
549 tive to $\phi(x, y)$.

550 In the discrete case, where s, ϕ are not given as continuous sur-
551 faces, but are represented by a mesh in equilibrium and its Airy
552 mesh, we use the techniques of Schiftner [2007] and Cohen-Steiner
553 and Morvan [2003] to approximate the Hessians $\nabla^2 s, \nabla^2 \phi$, com-
554 pute principal directions as eigenvectors of $(\nabla^2 \phi)^{-1} \nabla^2 s$, and sub-
555 sequently find meshes \mathcal{S}, Φ approximating s, ϕ which follow those
556 directions. Global optimization now makes \mathcal{S}, Φ a valid thrust net-
557 work with discrete stress potential. Convexity of Φ ensures that \mathcal{S}
558 is self-supporting.

559 Note that the relative principal curvature directions give the *unique*
560 curve network along which a planar quad discretization of a self-
561 supporting surface is possible. Other networks lead to results like
562 the one shown by Figure 10. Figures 11 and 16 further illustrate the
563 result of applying this procedure to self-supporting surfaces.

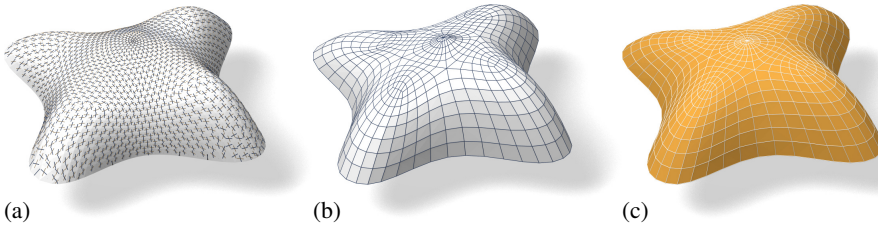


Figure 11: Planar quad remeshing of the “Lilium tower” surface of Figure 6. (a) Principal directions which are found as eigenvectors of $(\nabla^2\phi)^{-1}\nabla^2s$. (b) Quad mesh guided by principal directions is almost planar and almost self-supporting. (c) Small changes achieve both properties.

564 **Remark:** When remeshing a given shape by planar quad meshes, we
 565 know that the circular and conical properties require that the mesh
 566 follows the ordinary, Euclidean principal curvature directions [Liu
 567 et al. 2006]. It is remarkable that the self-supporting property in a
 568 similar manner requires us to follow certain *relative* principal direc-
 569 tions. Practitioners’ observations regarding the beneficial statics
 570 properties of principal directions can be explained by this analogy,
 571 because the relative principal directions are close to the Euclidean
 572 ones, if the stress distribution is uniform and $\|\nabla s\|$ is small.

573 **Koenigs Meshes.** Given a self-supporting thrust network \mathcal{S} with
 574 stress surface Φ , we ask the question: Which vertical perturbation
 575 $\mathcal{S} + \mathcal{R}$ is self-supporting, with the same loads as \mathcal{S} ? As to notation,
 576 all involved meshes $\mathcal{S}, \mathcal{R}, \Phi$ have the same top view, and arithmetic
 577 operations refer to the respective z coordinates s_i, r_i, ϕ_i of vertices.

578 The condition of equal loads then is expressed as $\Delta_\phi(s + r) =$
 579 $\Delta_\phi s$ in terms of Laplacians or as $H_{\mathcal{S}}^{\text{rel}} = H_{\mathcal{S} + \mathcal{R}}^{\text{rel}}$ in terms of mean
 580 curvature, and is equivalent to

$$\Delta_\phi r = 0, \quad \text{i.e.,} \quad H_{\mathcal{R}}^{\text{rel}} = 0.$$

581 So \mathcal{R} is a *minimal surface* relative to Φ . While in the triangle mesh
 582 case there are enough degrees of freedom for nontrivial solutions,
 583 the case of planar quad meshes is more intricate: Polar polyhedra
 584 \mathcal{R}^* , Φ^* have to be Christoffel duals of each other [Pottmann and
 585 Liu 2007], as illustrated by Figure 5. Unfortunately not all quad
 586 meshes have such a dual; the condition is that the mesh is *Koenigs*,
 587 i.e., the derived mesh formed by the intersection points of diagonals
 588 of faces again has planar faces [Bobenko and Suris 2008].



Figure 12: A “Koebe” mesh Φ is self-supporting for unit dead load. An entire family of self-supporting meshes with the same top view is defined by $\mathcal{S}_\alpha = \Phi + \alpha\mathcal{R}$, where \mathcal{R} is chosen as Φ ’s Christoffel-dual.

589 **Koebe meshes.** An interesting special case occurs if Φ is a
 590 *Koebe mesh* of isotropic geometry, i.e., a PQ mesh whose edges
 591 touch the Maxwell paraboloid. Since Φ approximates the Maxwell
 592 paraboloid, we get $2K(\mathbf{v}_i)H^{\text{rel}}(\mathbf{v}_i) \approx 1$ and Φ consequently is
 593 self-supporting for unit load. Applying the Christoffel dual con-
 594 struction described above yields a minimal mesh \mathcal{R} and a family of
 595 meshes $\Phi + \alpha\mathcal{R}$ which are self-supporting for unit load (see Fig-
 596 ure 12).

6 Conclusion and Future Work

598 **Conclusion.** This paper builds on relations between statics and
 599 geometry, some of which have been known for a long time, and

600 connects them with newer methods of discrete differential geom-
 601 etry, such as discrete Laplace operators and curvatures of polyhedral
 602 surfaces. We were able to find efficient ways of modeling self-sup-
 603 porting freeform shapes, and provide architects and engineers with
 604 an interactive tool which gives quick information on the statics of
 605 freeform geometries. The self-supporting property of a shape is di-
 606 rectly relevant for freeform masonry. The actual thrust networks we
 607 use for computation are relevant e.g. for steel constructions, where
 608 equilibrium of deadload forces implies absence of moments. This
 609 theory and accompanying algorithms thus constitute a new contri-
 610 bution to architectural geometry, connecting statics and geometric
 611 design.

612 **Future Work.** There are several directions of future research. One
 613 is to incorporate non-manifold meshes, which occur naturally when
 614 e.g. supporting walls are introduced. It is also obvious that non-ver-
 615 tical loads, e.g. wind load, play a role. There are also some direc-
 616 tions to pursue in improving the algorithms, for instance adaptive
 617 remeshing in problem areas. Probably the interesting connections
 618 between statics properties and geometry are not yet exhausted, and
 619 we would like to propose the *geometrization* of problems as a strat-
 620 egy for their solution.

References

- 621 ASH, P., BOLKER, E., CRAPO, H., AND WHITELEY, W. 1988.
 622 Convex polyhedra, Dirichlet tessellations, and spider webs. In
 623 *Shaping space* (Northampton, Mass., 1984). Birkhäuser, Boston,
 624 231–250.
- 626 BARNES, M. R. 2009. Form finding and analysis of tension struc-
 627 tures by dynamic relaxation. *Int. J. Space Structures* 14, 2, 89–
 628 104.
- 629 BLOCK, P., AND LACHAUER, L. 2011. Closest-fit, compression-
 630 only solutions for free form shells. In *IABSE — IASS 2011 Lon-
 631 don Symposium*, Int. Ass. Shell Spatial Structures. electronic.
- 632 BLOCK, P., AND OCHSENDORF, J. 2007. Thrust network analysis:
 633 A new methodology for three-dimensional equilibrium. *J. Int.
 634 Assoc. Shell and Spatial Structures* 48, 3, 167–173.
- 635 BLOCK, P. 2009. *Thrust Network Analysis: Exploring Three-
 636 dimensional Equilibrium*. PhD thesis, Massachusetts Institute
 637 of Technology.
- 638 BOBENKO, A., AND SURIS, YU. 2008. *Discrete differential geom-
 639 etry: Integrable Structure*. No. 98 in Graduate Studies in Math.
 640 American Math. Soc.
- 641 BOBENKO, A., POTTMANN, H., AND WALLNER, J. 2010. A
 642 curvature theory for discrete surfaces based on mesh parallelity.
 643 *Math. Annalen* 348, 1–24.
- 644 COHEN-STEINER, D., AND MORVAN, J.-M. 2003. Restricted
 645 Delaunay triangulations and normal cycle. In *Proc. 19th Symp.
 646 Computational geometry*, ACM, 312–321.

- 647 FRATERNALI, F., ANGELILLO, M., AND FORTUNATO, A. 2002. 702 SCHIFTNER, A. 2007. *Planar quad meshes from relative principal
648 A lumped stress method for plane elastic problems and the 703 curvature lines.* Master's thesis, TU Wien.
649 discrete-continuum approximation. *Int. J. Solids Struct.* 39,
650 6211–6240.
- 651 FRATERNALI, F. 2010. A thrust network approach to the equi- 704 SORKINE, O., COHEN-OR, D., AND TOLEDO, S. 2003. High-
652 librium problem of unreinforced masonry vaults via polyhedral 705 pass quantization for mesh encoding. In *Symposium Geometry
653 stress functions. *Mechanics Res. Comm.* 37, 2, 198 – 204.*
- 654 FRIEDLANDER, M. P., 2007. BCLS: Bound constrained least 706 VAN MELE, T., AND BLOCK, P. 2011. A novel form finding
655 squares. <http://www.cs.ubc.ca/~mpf/bcls>. 707 method for fabric formwork for concrete shells. *J. Int. Assoc.
656 GIAQUINTA, M., AND GIUSTI, E. 1985. Researches on the equi- 708 Shell and Spatial Structures* 52, 217–224.
- 657 librium of masonry structures. *Archive for Rational Mechanics
658 and Analysis* 88, 4, 359–392.
- 659 GLYMPH, J., SHELDEN, D., CECCATO, C., MUSSEL, J., AND 709 WARDETZKY, M., MATHUR, S., KÄLBERER, F., AND GRIN-
660 SCHOBER, H. 2004. A parametric strategy for free-form glass 710 SPUN, E. 2007. Discrete Laplace operators: No free lunch.
661 structures using quadrilateral planar facets. *Automation in Con- 711 In *Symposium on Geometry Processing*, A. Belyaev and M. Gar-
662 struction* 13, 2, 187 – 202.
- 663 HEYMAN, J. 1966. The stone skeleton. *Int. J. Solids Structures* 2, 712 WHITING, E., OCHSENDORF, J., AND DURAND, F. 2009. Proce-
664 249–279.
- 665 HEYMAN, J. 1995. *The Stone Skeleton: Structural Engineering of 713 masonry Architecture.* Cambridge University Press.
- 666 HEYMAN, J. 1998. *Structural Analysis: A Historical Approach.* 714 Cambridge University Press.
- 667 KILIAN, A., AND OCHSENDORF, J. 2005. Particle-spring sys-
668 tems for structural form finding. *J. Int. Assoc. Shell and Spatial
669 Structures* 46, 77–84.
- 670 LIPMAN, Y., SORKINE, O., COHEN-OR, D., LEVIN, D., ROSSI, 715
671 C., AND SEIDEL, H. 2004. Differential coordinates for interac-
672 tive mesh editing. In *Proc. SMI. IEEE*, 181–190.
- 673 LIU, Y., POTTMANN, H., WALLNER, J., YANG, Y.-L., AND 716
674 WANG, W. 2006. Geometric modeling with conical meshes
675 and developable surfaces. *ACM Trans. Graph.* 25, 3, 681–689.
676 Proc. SIGGRAPH.
- 677 LIVESLEY, R. K. 1992. A computational model for the limit anal- 717
678 ysis of three-dimensional masonry structures. *Meccanica* 27,
679 161–172.
- 680 MAXWELL, J. 1864. On reciprocal diagrams and diagrams of 718
681 forces. *Philosophical Magazine* 4, 27, 250–261.
- 682 O'Dwyer, D. 1998. Funicular analysis of masonry vaults. *Com- 719
683 puters and Structures* 73, 187–197.
- 684 PAIGE, C. C., AND SAUNDERS, M. A. 1975. Solution of sparse 720
685 indefinite systems of linear equations. *SIAM Journal on Numer-
686 ical Analysis* 12, 617–629.
- 687 POTTMANN, H., AND LIU, Y. 2007. Discrete surfaces in isotropic 721
688 geometry. In *Mathematics of Surfaces XII*, M. Sabin and J. Win-
689 kler, Eds., vol. 4647 of *LNCS*. Springer-Verlag, 341–363.
- 690 POTTMANN, H., LIU, Y., WALLNER, J., BOBENKO, A., AND 722
691 WANG, W. 2007. Geometry of multi-layer freeform structures
692 for architecture. *ACM Trans. Graphics* 26, 3, #65,1–11. Proc.
693 SIGGRAPH.
- 694 SCHEK, H.-J. 1974. The force density method for form finding and 723
695 computation of general networks. *Computer Methods in Applied
696 Mathematics and Engineering* 3, 115–134.
- 697 SCHIFTNER, A., AND BALZER, J. 2010. Statics-sensitive layout 724
698 of planar quadrilateral meshes. In *Advances in Architectural Ge-
699 ometry 2010*, C. Ceccato et al., Eds. Springer, Vienna, 221–236.

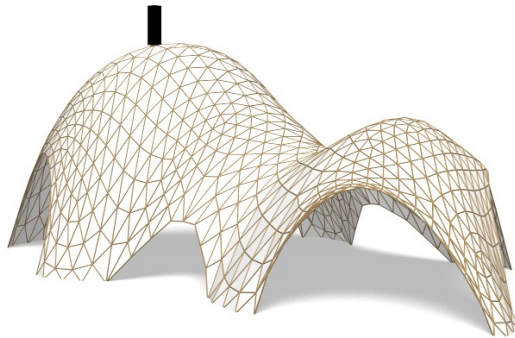


Figure 13: Testing stability. This self-supporting surface of length 24 m is imagined as masonry of thickness 0.1 m. It possesses a thrust network inside the masonry hull if, say, a load of 900 kg (shown in black) is applied to a certain vertex. This means that the surface is still stable after that load is applied (N.B. Our test is rather conservative).

Figure 14: Test sequence: Stability w.r.t. removal of single pieces of masonry. (a) self-supporting surface and thrust network. (b) Part of the surface has been removed, the existence of a modified thrust network shows it is self-supporting. (c) If we remove too much, our algorithm no longer finds an admissible thrust network. It is plausible that the surface is no longer self-supporting.

Figure 15: Structural Glass. Glass as a structural element can support stresses up to **FILL IN VALUES**. (a) Self-supporting thrust network such that forces do not exceed F_{\max} . (b) Remeshing of this surface by a planar quad mesh (not necessarily self-supporting). (c) A steel/glass construction following this quad mesh, which utilizes the structural properties of glass. Since it is very close to a self-supporting shape, joints will experience low bending and torsion moments.

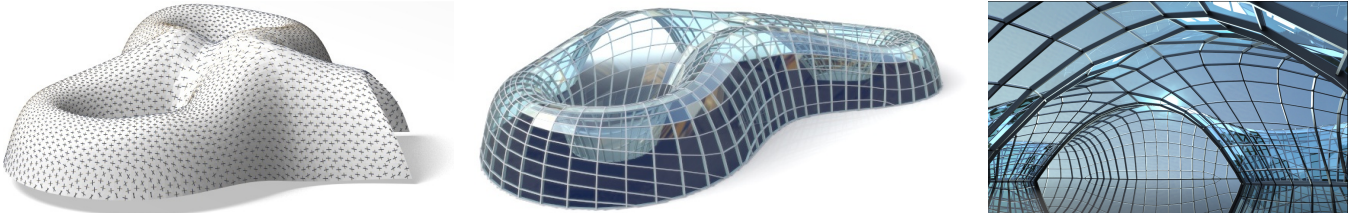


Figure 16: Planar quad remeshing of the surface of Figure 8. Left: Principal directions. Center: The result of optimization is a self-supporting PQ mesh, which guides a moment-free steel/glass construction. Right: Interior view.

Table 1: Numerical Data for Examples

Example	Figure	Vertices	Edges	Time (s)	Iterations	Max Rel Error
Top of Lilium Tower	Fig. 6, left	1201	3504	21.6	9	4.2×10^{-5}
Top of Lilium Tower (with pillar)	Fig. 6, right	1200	3500	26.5	10	8.5×10^{-5}
Freeform Structure with Two Pillars	Fig. 8	1535	2976	17.0	21	2.7×10^{-5}
Swiss Cheese	Fig. 9	2358	4302	19.5	9	3.0×10^{-4}
Brick Domes	Fig. 14	752	2165	8.0	9	5.8×10^{-5}
Structural Glass	Fig. 15	527	998	5.7	25	2.4×10^{-5}

Table 2: Numerical details about the examples throughout this paper. Time: The wall-clock time needed by an Intel Xeon 2.3GHz desktop PC with 4 GB of RAM to find a self-supporting thrust network and associated stress surface from the example's reference mesh; this optimization required Iterations outer iterations of the four steps in (§3). Max Rel Error: The maximum, over interior thrust network vertices i , of the dimensionless relative error in force equilibrium $\left\| A_i F_i - \sum_{j \sim i} w_{ij} (\mathbf{v}_j - \mathbf{v}_i) \right\| / \| A_i F_i \|$.